Available online at www.sciencedirect.com

SciVerse ScienceDirect

Geochimica et Cosmochimica Acta 84 (2012) 525–533

Geochimica et Cosmochimica Acta

www.elsevier.com/locate/gca

Evaluation of isotopic fractionation of oxygen ions escaping from terrestrial thermosphere

Yasutaka Hiraki [a,*], Akinori Yamada [b], Yasuko Kasai [c], Takamasa Seta [c], Minoru Ozima [b]

[a] National Institute for Fusion Science, Oroshi-cho 322-6, Toki, Gifu 509-5292, Japan
[b] Department of Earth and Planetary Science, University of Tokyo, Tokyo, Japan
[c] National Institute of Information and Communications Technology (NICT), Tokyo, Japan

Received 5 July 2011; accepted in revised form 7 February 2012; available online 22 February 2012

Abstract

Oxygen isotopic ratios in contemporary lunar soils indicate a highly mass-independent fractionation (MIF) of $\Delta^{17}O \approx 25$ per mil. This fraction is comparable to the ratio for stratospheric ozone and is thus supposed to have originated from the terrestrial upper atmosphere through transport of oxygen ions by the intense Earth wind. In this paper, we develop a one-dimensional chemical model that can solve for the ionic and neutral compositions of oxygen isotopes by including the isotopic effects in dynamical, photolytic, and chemical processes. We first confirm that the isotopic ratios of O^+, O_2^+, O, and O_2 are nearly mass dependent, $\Delta^{17}O \approx 0$ per mil, when the isotopic effects of multiple (eddy, molecular, and ambipolar) diffusion processes are taken into account. We examine which photolytic and chemical processes can produce a strong MIF for oxygen species and select four candidates: photo-dissociative ionization of O_2, photo-dissociation of O_2 by Lyman-α solar emissions, charge exchange between O^+ and O_2^+, and atomic exchanges between O and O_2. We estimated the oxygen isotopic ratio to be $\Delta^{17}O \approx 1$–4 per mil at the height of 100–400 km on the basis of a statistical treatment of atom mechanics. These values are smaller than those in the lunar case, and we conclude that a more rigorous quantum mechanical treatment of photo-dissociation processes will be necessary before we can make an evaluation of the role of Earth-escaping oxygen isotopes.

1. INTRODUCTION

Oxygen is the third most abundant element in the solar system and it is one of the most crucial aspects to understanding evolution of the system. However, its mean elemental and isotopic compositions are still not well understood (cf. Clayton, 2002a,b; Yurimoto and Kuramoto, 2004; Lyons and Young, 2005; Hashizume and Chaussidon, 2005; Ozima et al., 2007). Recent measurements of contemporary lunar soils have indicated that the oxygen isotopic ratio in the metallic particles has a highly mass-independent fractionation (MIF) of $\Delta^{17}O \approx 25$ per mil (Ireland et al., 2006). There is also a negative anomaly in the same metal grains as well, thus the value remains controversial. Here, $\Delta^{17}O = \delta^{17}O - 0.52\ \delta^{18}O$ stands for the strength of MIF where $\delta^{n}O = \{([^{n}O]/[^{16}O])/([^{n}O]/[^{16}O])_{SMOW} - 1\} \times 10^3$ in per mil with $n = 17$ or 18; the density ratio denoted by "SMOW" means the Standard Mean Ocean Water content. Ireland et al. (2006) emphasized that this value must be indigenous to the solar wind-implanted component and accordingly it represents the mean isotopic ratio of the solar system. Two predictions have thus far been made for the mean value of $\Delta^{17}O$; one predicts a negative MIF of -20 per mil (Clayton, 2002a; Hashizume and Chaussidon, 2005; Lyons and Young, 2005), and another predicts $\Delta^{17}O = 0$ per mil (Ozima et al., 2007). The measured lunar oxygen isotopic ratio can be taken as a third prediction. This exotic oxygen has roughly the same isotopic ratio as is commonly found in the terrestrial atmosphere in stratospheric nitric oxides and ozone (Thiemens, 2006; and references

* Corresponding author.
E-mail address: hiraki.yasutaka@nifs.ac.jp (Y. Hiraki).

0016-7037/$ - see front matter © 2012 Elsevier Ltd. All rights reserved.
doi:10.1016/j.gca.2012.02.010

therein). These facts motivated us to study if the exotic oxygen could be attributable to the Earth-escaping wind, as suggested by our previous studies (Ozima et al., 2007, 2008; Hiraki et al., 2008b). This would be the first attempt to assess the direct interaction between the terrestrial atmosphere and the lunar surface, which in turn would yield a new means to trace the evolution of oxygen in the terrestrial atmosphere.

Such speculation is supported by recent observations of the Earth-escaping ion flow by the GEOTAIL mission (Seki et al., 2001). Since the ambient magnetic field line opens in the high latitude (cusp) region, a measurable amount of energetic oxygen ions O^+ can escape Earth's gravitation and reach far beyond lunar orbit. Seki et al. (2001) estimated the escaping O^+ flux at the lunar orbit, and the flux of O that hits the surface is $\approx 3.7 \times 10^3$ cm^{-2} s^{-1}. Their numerical simulations indicate that the escaping O^+ flux is more or less consistent with the amount of the exotic oxygen implanted in metallic particles. If the MIF of exotic oxygen originates from the present-day Earth, this would give robust support for the Earth-wind hypothesis. Another problem is whether the implantation process on the Moon can change the oxygen isotopic ratio, but this is beyond our present scope.

The lunar surface is exposed to the solar wind as well as the Earth wind. There are a few estimates of the solar-wind oxygen flux in interplanetary space (e.g. von Steiger et al., 2000; Hashizume and Chaussidon, 2005). Taking the average abundance ratio of He/O and assuming the shielding factor of the geomagnetic tail, the O flux at the lunar surface was estimated to be 1.5×10^4 cm^{-2} s^{-1}, which is a factor of four larger than the estimated Earth-wind O flux. If the solar-wind O has a different value of $\Delta^{17}O$ from the Earth-wind O, the oxygen isotopic signature of the Earth wind would be diluted by a factor of five; note that the dilution rate depends on the Earth wind conditions and the solar activity. In order for our hypothesis to be tenable, the $\Delta^{17}O$ values in the Earth atmosphere should be at least comparable to those observed for exotic oxygen.

Numerical studies were made to estimate the isotopic fractionation rates of oxygen for minor species in the middle atmosphere (e.g. Lyons, 2001; Zahn et al., 2006; Liang et al., 2007). These estimates showed maximum values of $\Delta^{17}O = 30$–80 per mil for NO_x, HO_2, H_2O, OH, and O_3 in the stratosphere (20–30 km). It was also found that the MIF ratio of oxygen inversely correlates with concentrations of nitrous oxide and methane since these molecules are sinks for the reactions related to the above minor species. Direct observations of CO_2 have been made using balloons, rockets, and aircraft (e.g. Boering et al., 2004; Thiemens, 2006; and references therein). The estimated $\Delta^{17}O$ is ≈ 10 per mil for CO_2 and 40–60 per mil for O_3 in the stratosphere. Laboratory analyses showed that the oxygen isotopic ratio of the sampled CO_2 linearly increases with altitude up to $\Delta^{17}O \approx 12$ per mil at 60 km, which suggests even higher values at higher altitudes (Thiemens et al., 1995). However, because of the low abundance of CO_2 in the upper atmosphere, this ratio may not be directly relevant to the isotopic signature of the Earth-wind oxygen. Thiemens' group intends to gather information on oxygen in the middle atmosphere (90–110 km) with their latest rocket measurements.

In spite of the vigorous measurements on light oxygen ($\Delta^{17}O > 0$), the current information on the isotopic composition that is available from measurements and theoretical calculations is limited to less than 100 km and is not useful for assessing the isotopic characteristics of the Earth-wind O. The purpose of our study is to determine if the origin of the large MIF of lunar oxygen is the terrestrial upper atmosphere. We focused on the high-latitude thermosphere (100–300 km) where oxygen ions start to escape. We developed an ion-neutral chemical model that includes oxygen isotopes for atmospheric minor species such as O^+. We calculated the amount and the sign of the isotopic ratios $\Delta^{17}O$ and clarified the source mechanisms (see Section 2.1). The MIF for neutral major species of O_2 can largely affect ionic species; as a result, composition changes in major neutral species are self-consistently treated in this model. In Section 2.2, we present a test calculation including the isotopic effect of multiple (eddy, molecular, and ambipolar) diffusion coefficients. In Section 3.1, we assess the key photolytic and chemical processes in the altitude range of 100–300 km and determine the candidates that can produce a large MIF. In Section 3.2, we perform several test simulations including the isotopic effects of the photolytic and chemical reaction coefficients. We present estimates for isotopes in the upper atmosphere based on a statistical treatment of atomic reaction mechanics.

Before showing the details of our chemical model, we briefly mention recent studies on the generation of large MIFs due to chemical reactions or photolyses. Gao and Marcus (2001) proposed a semi-empirical theory based on measured isotope-specific rate coefficients for the formation of O_3 that explains the observed large MIF ratios for stratospheric ozone. They pointed out that the reaction speed difference due to the asymmetry of O_3 isotopes leads to a large MIF. Lyons and Young (2005) suggested a self-shielding effect in photo-dissociation of CO molecules in the solar nebula. Navon and Wasserburg (1985) examined the self-shielding effect of photo-dissociation of O_2 in oxygen-rich low pressure gas and found that it cannot occur in the nebula because of the rapidity of isotope exchange. Similar processes would be expected in the upper atmosphere, owing to the chemical reactions associated with $\geqslant 3$ oxygens or photolysis in the ultraviolet wavelength range.

2. CHEMICAL MODEL OF OXYGEN ISOTOPES

2.1. Model description

We will start with an outline of our chemical model and simulation conditions. The model included species that contain only one oxygen isotope, e.g. $^{16}O^{17}O^+$ and $^{16}O^{18}O^+$, but no species with two or more isotopes such as $^{17}O^{17}O^+$ in the case of O_2^+. We took into account the 150 reactions summarized in Table 1 by referring to the JPL94 data compilation (DeMore et al., 1994) for neutral–neutral reactions and by referring to Mätzing (1991) for ion-neutral reactions. We included the photo-ionization processes shown

Table 1
Reactions and rate coefficients included in our model; M is a catalyst, T is the neutral temperature. The coefficients are in units of $cm^3\ s^{-1}$, while those labeled by $*$ in units of $cm^6\ s^{-1}$. The value labeled by $**$ is taken from Anderson et al. (1985). The right column lists the total number of reaction paths for oxygen isotopic components. The label "–" means a reaction that has no isotopic component.

No.	Reaction	Rate coefficient	Incl. O isotope
R1	$N^+ + N_2 \rightarrow N_2^+ + N$	2.55×10^{-10}	–
R2	$N^+ + O_2 \rightarrow O^+ + NO$	4.64×10^{-11}	5
R3	$N^+ + O_2 \rightarrow O_2^+ + N$	3.07×10^{-10}	3
R4	$N^+ + O_2 \rightarrow NO^+ + O$	2.6×10^{-10}	5
R5	$N^+ + O \rightarrow O^+ + N$	1.0×10^{-12}	3
R6	$N^+ + O + M \rightarrow NO^+ + M$	$1.0 \times 10^{-29}(300/T)*$	3
R7	$N^+ + N + M \rightarrow N_2^+ + M$	$1.0 \times 10^{-29}(300/T)*$	–
R8	$N^+ + NO \rightarrow NO^+ + N$	4.1×10^{-10}	3
R9	$N^+ + NO \rightarrow N_2^+ + O$	5.0×10^{-11}	3
R10	$N^+ + e \rightarrow N$	$3.5 \times 10^{-12}(300/T)^{0.7}$	–
R11	$N_2^+ + O \rightarrow O^+ + N_2$	9.8×10^{-12}	3
R12	$N_2^+ + O_2 \rightarrow O_2^+ + N_2$	$3.9 \times 10^{-10}\exp(-T/143)$	3
R13	$N_2^+ + O_2 \rightarrow NO^+ + NO$	1.0×10^{-17}	5
R14	$N_2^+ + O \rightarrow NO^+ + N$	2.1×10^{-10}	3
R15	$N_2^+ + NO \rightarrow NO^+ + N_2$	3.3×10^{-10}	3
R16	$N_2^+ + N \rightarrow N^+ + N_2$	1.0×10^{-11}	–
R17	$N_2^+ + e \rightarrow N + N$	$2.2 \times 10^{-7}(300/T)^{0.39}$	–
R18	$N_2^+ + e \rightarrow N_2$	$4.0 \times 10^{-12}(300/T)^{0.7}$	–
R19	$O^+ + O_2 \rightarrow O_2^+ + O$	$6.6 \times 10^{-10}T^{-0.55}$	9 (21)
R20	$O^+ + N_2 \rightarrow N_2^+ + O$	$9.0 \times 10^{-11}T^{-0.7}$	3
R21	$O^+ + N_2 \rightarrow NO^+ + N$	1.2×10^{-12}	3
R22	$O^+ + NO \rightarrow NO^+ + O$	1.0×10^{-12}	5
R23	$O^+ + e \rightarrow O$	$4.0 \times 10^{-12}(300/T)^{0.7}$	3
R24	$O_2^+ + N_2 \rightarrow NO^+ + NO$	1.0×10^{-16}	5
R25	$O_2^+ + N \rightarrow NO^+ + O$	1.8×10^{-10}	5
R26	$O_2^+ + NO \rightarrow NO^+ + O_2$	3.5×10^{-10}	5 (9)
R27	$O_2^+ + e \rightarrow O + O(^1D)$	$2.1 \times 10^{-7}(300/T)^{0.55}$	5
R28	$O_2^+ + e \rightarrow O_2$	$4.0 \times 10^{-12}(300/T)^{0.7}$	3
R29	$NO^+ + e \rightarrow N + O$	$4.3 \times 10^{-7}(300/T)^{0.80}$	3
R30	$NO^+ + e \rightarrow NO$	$4.0 \times 10^{-12}(300/T)^{0.70}$	3
R31	$H^+ + O \rightarrow O^+ + H$	3.75×10^{-10}	3
R32	$H^+ + O_2 \rightarrow O_2^+ + H$	1.17×10^{-9}	3
R33	$H^+ + e \rightarrow H$	$1.9 \times 10^{-10}T^{-0.7}$	–
R34	$O + O + M \rightarrow O_2 + M$	$4.7 \times 10^{-33}(300/T)^{2.0}$	3
R35	$O_2 + O \rightarrow O_2 + O$	2.9×10^{-12} **	4 (6)
R36	$O_2 + N \rightarrow NO + O$	$1.5 \times 10^{-11}\exp(-3600/T)$	5
R37	$NO + N \rightarrow N_2 + O$	$2.1 \times 10^{-11}\exp(-100/T)$	3
R38	$O(^1D) + N_2 \rightarrow O + N_2$	$1.8 \times 10^{-11}\exp(110/T)$	3
R39	$O(^1D) + O_2 \rightarrow O + O_2$	$3.2 \times 10^{-11}\exp(70/T)$	9

in Table 2; the cross sections and the solar irradiance intensity in the wavelength range of 7.5–102.5 nm were taken from the EUVAC model (Richards et al., 1994). Our model

Table 2
Photoionization processes included in our model. Definitions of the rate coefficients are given in the text. The meanings of the number and "–" in right column are the same as in Table 1.

No.	Reaction	Incl. O isotope
J1	$N_2 + h\nu \rightarrow N_2^+ + e$	–
J2	$N_2 + h\nu \rightarrow N^+ + N + e$	–
J3	$N + h\nu \rightarrow N^+ + e$	–
J4	$O_2 + h\nu \rightarrow O_2^+ + e$	3
J5	$O_2 + h\nu \rightarrow O^+ + O + e$	5, Incl. $O(^1D)$
J6	$O + h\nu \rightarrow O^+ + e$	3
J7	$H + h\nu \rightarrow H^+ + e$	–

is basically the same as a classical one-dimensional model for thermospheric chemistry studies (e.g. Ogawa and Shimazaki, 1975). We solve 28 sets of photochemical equations for ionic and neutral species including oxygen isotopes (^{17}O and ^{18}O) and electrons,

$$\frac{\partial [X_i]}{\partial t} = P_i - L_i[X_i] + \frac{\partial}{\partial z}\left[D\left\{\frac{\partial [X_i]}{\partial z} + \left(\frac{1}{T}\frac{\partial T}{\partial z} + \frac{1}{H_i}\right)[X_i]\right\}\right] \quad (1)$$

where $[X_i]$ is the density of species X_i, P_i and L_i are the production and loss rates, D is the diffusion coefficient (see Section 2.2), T is the air temperature, and $H_i = kT/(m_i g)$ is the scale height with the mass m_i of species X_i; k is the Boltzmann constant, and g is the gravitational constant. The calculation domain is set in the altitude range of $z = 100$–1500 km.

Now let us briefly explain the numerical techniques for solving Eq. (1). Chemical reactions are treated by an

implicit scheme similar to what we did in our previous study (Hiraki et al., 2008a). For spatial integration of the diffusion term, we assume a fixed boundary condition at the bottom $z = 100$ km of the system and the flux-controlled boundary condition (Ogawa and Shimazaki, 1975) at the top $z = 1500$ km. To benchmark the accuracy of our calculation, we solved the coupled Eq. (1) with $D = 0$ for all species and confirmed 8–9 orders of accuracy for the local mass conservation of N, ^{16}O, ^{17}O, ^{18}O, and H. Thus, this model can sufficiently resolve the MIF of oxygen ions in the range of 100–300 km.

We took the MSIS-E90 empirical model data for the initial density and temperature profiles of ^{16}O-containing neutral species at the latitude of 75°. This latitude corresponds to the cusp region where strong ion outflow appears. We assumed low solar activity where the F10.7-irradiance intensity is 80. The air temperature is $T \approx 200$, 830, and 900 K at altitudes of 100, 200, and >300 km, respectively. Using the ^{16}O-containing neutral densities and the SMOW isotope ratio of $[^{16}O] : [^{17}O] : [^{18}O] = 99.763 : 0.037 : 0.200$, we determined the initial values of ^{17}O- and ^{18}O-containing neutral densities so that the oxygen isotope ratio would be $\Delta^{17}O = 0$ per mil for all neutral species. The initial densities of all ions are set to zero, and the steady-state solution was confirmed to be independent of the initial values. We performed a time integration of Eq. (1) to $t = 50$ h in order to obtain the steady-state solution of the ion and neutral densities by setting the local time at noon.

2.2. Dynamical effects

Molecular and eddy diffusion are taken into account as dynamical effects on neutral species, while ambipolar diffusion is included in the continuity Eq. (1) of ions. The molecular diffusion coefficient D_m is defined by the Chapman–Enskog theory as

$$D_m = \frac{3}{8N\sigma_0}\sqrt{\frac{kT(m+M)}{2\pi mM}}, \tag{2}$$

where N, M, and T are the atmospheric density, average mass, and temperature, respectively, m is the target particle mass, and $\sigma_0 \approx 10^{-15}$ cm^2 is a parameter defined from the collision integral and molecular radius. The coefficient mainly has a dependence on N^{-1} and $D_m \approx 10^6$, 10^{10}, and 10^{14} cm^2/s at $z = 100$, 300, and 800 km, respectively. Ogawa and Shimazaki (1975) give the functional dependence of the eddy diffusion coefficient as

$$K = \begin{cases} K_1 \exp(-s_1\bar{z}^2) & (\bar{z} = z - z_0 > 0) \\ (K_1 - K_2)\exp(-s_1\bar{z}^2) + K_2 \exp(s_2\bar{z}) & (\bar{z} \leqslant 0) \end{cases} \tag{3}$$

where $K_1 = 10^7$ and $K_2 = 2 \times 10^6$ in units of cm^2/s, $s_1 = 0.05$ and $s_2 = 0.07$ in units of km^{-1}, and $z_0 = 100$ km for the turbopause height. It is found from the values of K_1 and K_2 that the eddy diffusion dominates the molecular diffusion below the height of ≈110 km. The ambipolar diffusion coefficient for ions is defined as $D_a = D_m(1 + T_e/T_i)$ using the molecular diffusion coefficient and the ion and electron temperatures. The temperature profiles are taken from the International Reference Ionosphere (IRI) 2000 model (Bilitza, 2001). In our setting, the temperature ratio T_e/T_i peaks at $z \approx 300$ km and D_a is three times larger than D_m there.

Using these diffusion coefficients, we performed a calculation to validate our model and to identify the key reactions at the altitudes of interest. Here, the chemical reaction does not include an isotopic effect. Fig. 1 shows the altitude distribution of the densities for major ionic and neutral species and our model produced realistic profiles. The compositions of O^+, O_2^+, and NO^+ at 100–300 km are consistent with those in the IRI model. The compositions of major neutral species as well as NO have realistic profiles. Furthermore, the altitude dependence for the isotopic species denoted by $Q \equiv {}^{17}O + {}^{18}O$ is sufficiently resolved.

We investigated the effect of the multiple diffusion processes on the oxygen isotopic ratio $\Delta^{17}O$, as regards the hypothesis that non-mass dependent factors such as eddy (K) and ambipolar ($D_a \sim 1 + T_e/T_i$) diffusion cause the MIF of O-containing species. Fig. 2 shows the altitude distribution of $\Delta^{17}O$ for O^+, O_2^+, O, and O_2 at 100–800 km for the calculation in Fig. 1. The values of $\Delta^{17}O$ are less than 1 per mil in the altitude range of interest. It is not shown but, when we artificially eliminated the ambipolar effect ($D_a = 0$), the amplitude of $\Delta^{17}O$ became less than ±0.2 per mil for all species shown. In particular, $\Delta^{17}O \approx 10^{-3}$ per mil for O^+. While these results imply the range of numerical errors for the long time integration, they show

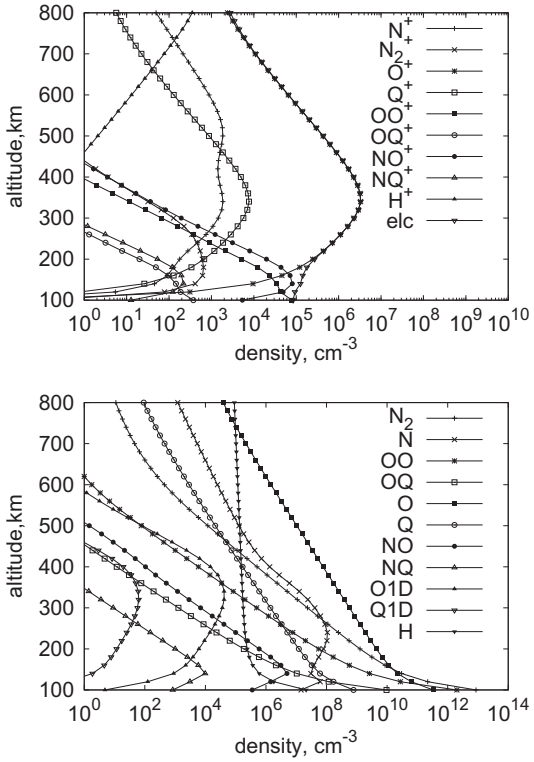

Fig. 1. Altitude distributions of major ion densities (top) and neutral densities (bottom) including oxygen isotopic components at $t = 50$ h; $Q \equiv {}^{17}O + {}^{18}O$.

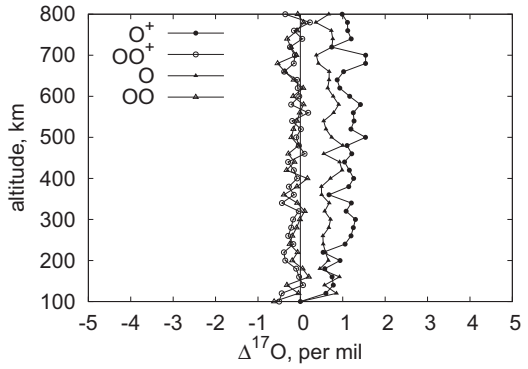

Fig. 2. Oxygen isotopic ratio $\Delta^{17}O$ for oxygen-containing species O^+, O_2^+, O, and O_2 at $t = 50$ h and taking into account only the isotopic effect of the multi-diffusion processes.

that the eddy process causes no MIF. Because the lower boundary condition is severe, $\Delta^{17}O = 0$ per mil, it does not have a noticeable effect on any species. A weak positive $\Delta^{17}O \approx 1$ per mil for O^+ and O is produced by inclusion of ambipolar diffusion. However, it also seems to be due to numerical errors, mainly from the upper rarefied atmosphere, because the effect of the ambipolar process should be at a maximum at $z \approx 300$ km where D_a peaks. In spite of these elaborate studies, we conclude that these diffusion processes do not cause MIF. In the analysis hereafter, we eliminate the ambipolar diffusion term ($D_a = 0$) and examine the isotopic effects of the key chemical reactions in the thermosphere. An isotopic change larger than 1 per mil can be analyzed with this model.

3. PHOTOLYTIC AND CHEMICAL EFFECTS

3.1. Selection of key processes

In this section, we investigate the key processes of thermospheric ion chemistry; the isotopic effects of these reactions will be examined later. We selected the dominant source and loss reactions for O^+ and O_2^+ at 150 and 300 km from Fig. 1 ($\Delta^{17}O \approx 0$ per mil for all species). The major sources of O^+ at 150 km are J6 (10^3), R11 (69), and J5 (28), while the major losses are R19 (10^{-2}), R21 (10^{-2}), and R20 (7×10^{-3}); the process numbers correspond to what is shown in Tables 1 and 2. The values in parentheses mean the production rate P in units of $cm^{-3}\ s^{-1}$, or the loss rate L in units of s^{-1}. For O_2^+, the sources are R19 (463), J4 (118), and R3 (15), while the losses are R27 (1.8×10^{-2}), R25 (6×10^{-3}), and R26 (10^{-3}). The major sources of O^+ at 300 km are J6 (140), R5 (0.8), and R11 (0.7), while the major losses are R21 (2.8×10^{-5}), R20 (1.8×10^{-5}), and R19 (7×10^{-6}). For O_2^+, the sources are R19 (17), J4 (0.24), and R3 (0.22), while the losses are R27 (0.26) and R25 (7×10^{-3}). The rates of other processes are much smaller than these.

We guessed that reactions associated with <3 oxygens result in a mass-dependent fractionation because the transition states are asymmetric only such as $^{16}O^{18}ON^+$ in R25. In this case, the reaction speed is mainly controlled by the mass difference between O and N. Thus, R3, R5, R11, R20, R21, R25, and R27 are eliminated as candidates that cause strong MIF. Although both R19 and R26 remains as candidates, we will consider here only the isotopic effect of the charge exchange R19; as we will see later, these processes are mass dependent. In the above selection, we ignored two neutral–neutral processes: atomic exchange between O and O_2 (R35) and photo-dissociation of O_2 by the Lyman-α (121.6 nm) solar emission. These processes control the isotopic balance of major neutral species O_2, and in turn, the oxygen isotopic ratios of neutrals can be converted into those of ionic species. In summary, we selected four processes for the evaluation of the isotopic effect, (1) photo-ionization J4–6, (2) photo-dissociation by Lyman-α, (3) charge exchange R19, and (4) atomic exchange R35.

Similar to the ozone isotope production suggested by Gao and Marcus (2001), it is expected that the reaction rate for R19 and R35 with an asymmetric state $^{16}O^{16}O^{18}O$ is faster than the rate with a symmetric transition state $^{16}O^{18}O^{16}O$. On the other hand, photolyses J4–6 and Lyman-α photo-dissociation should show some isotopic effects in atmospheric absorption. Note also that the branching process of O, $O(^1D)$, O^+, and their isotopes in J5 is assumed to be isotropic.

3.2. Evaluation of isotopic effects

We examined the isotopic effects of the four chemical reactions and photolyses selected in Section 3.1. Let us consider the isotopic effect of photoionization of O_2 (J4 and J5) and of O (J6). The previous theoretical and experimental studies focused on the photo-dissociation of O_2 (e.g., Liang et al., 2007). In general, photolytic processes may lead to isotopic fractionation when a strong perturbation happens between the inter-molecular potential curves of the rotational or vibrational electronic states. Furthermore, the zero point energy only plays a role in the case of dissociation such as J5. It is thus hard to see how the photoionizations J4 and J6 could cause isotopic fractionation because the mass of nuclei (or the number of neutrons) does not change the binding energy of the outermost electron. We performed a simple quantum chemical calculation to estimate the photo-dissociation cross sections of O_2 isotopes and used the results for the photo-dissociative ionization J5. We used the zero point energy model with the mirror image method proposed by Yung and Miller (1997) as a first approximation. A potential energy curve for one excited state of O_2 was calculated with the MRCI method, or the MOLPRO package (Werner and Knowles, 2006). The difference in the zero potential energies of the O_2 isotopes caused the difference in the cross sections of each absorption band. The absorption lines of $^{16}O^{17}O$ and $^{16}O^{18}O$ were red-shifted by ≈ 0.1 nm from those of $^{16}O^{16}O$. By assuming an O_2 temperature of 800 K, we find that the cross sections of J5 for $^{16}O^{17}O$ and $^{16}O^{18}O$ are 6 and 4 per mil smaller than that for $^{16}O^{16}O$.

We solved the chemical equation system (1) by putting these values into the rate coefficients of J5. The obtained $\Delta^{17}O$ values for O^+, O_2^+, O, and O_2 are shown in Fig. 3. As expected from the cross sections, the MIF ratio of

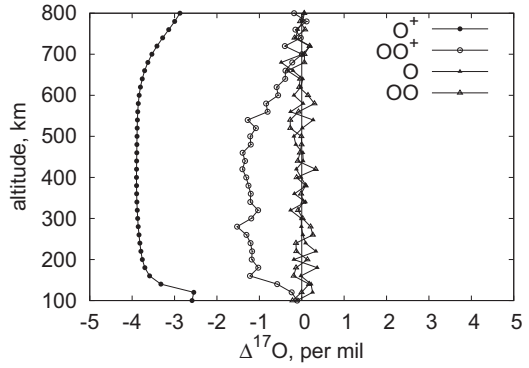

Fig. 3. Same as Fig. 2 except that the isotopic effect of the photo-dissociative ionization of O_2 labeled J5 is taken into account.

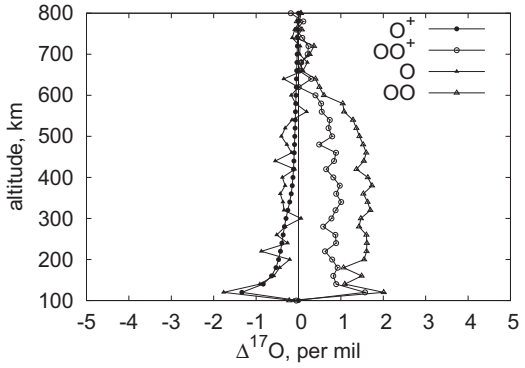

Fig. 4. Same as Fig. 2 except that the isotopic effect of the photo-dissociation of O_2 by Lyman-α (121.6 nm) is taken into account. A sharp drop around 100 km is due to the lower boundary condition at which the neutral densities are fixed.

$\Delta^{17}O \approx -3.8$ per mil is found for O^+ in a wide range of $z = 200$–650 km. The region where J5 is the source of O^+ is $z < 200$ km (see Section 3.1), but $\Delta^{17}O$ in higher altitudes show moderate MIFs owing to molecular diffusion of O_2. There is a weak MIF for O_2^+, $\Delta^{17}O \approx -1.2$ per mil, at $z = 150$–550 km. On the other hand, the isotopic ratios for neutrals O and O_2 are within the range of the numerical errors. We can consider that the isotopic ratio of O_2 is fully converted into an isotopic ratio of O^+, which is further converted into O_2^+ through the R19 charge exchange. Yamada et al. (2009) suggested that the mirror image method is not appropriate for oxygen molecules, and a more rigorous quantum calculation would show a still larger isotopic effect. Such a calculation should be done to investigate the photoionization of O_2 isotopes.

Next, we studied the isotopic effect of photo-dissociation of O_2 by Lyman-α solar radiation. Liang et al. (2007) computed the isotopic dependence of the O_2 dissociation cross section for Lyman-α using coupled-channel Schrödinger equation calculations. We used their cross section data for $^{16}O^{17}O$ and $^{16}O^{18}O$ at the right peak ($\approx$121.6 nm) of the Lyman-α solar spectrum with a background air temperature of 300 K; see Fig. 2 of their paper. The ratios of cross sections for $^{16}O^{17}O$ and $^{16}O^{18}O$ to that for normal O_2 was estimated to be $\approx$6 and $\approx$18, respectively. Referring to our previous study (Hiraki et al., 2008a), we defined the optical depth of O_2 at this wavelength as $10^{-20}N_{O_2} + 2.32 \times 10^{-18}N_{NO}$, where $N_i(z)$ is the total column density above a height z in units of cm^{-2}, and the solar irradiance of Lyman-α is 3.0×10^{11} $cm^{-2}\,s^{-1}$. Fig. 4 shows the results for the calculation including only this effect. Here, $\Delta^{17}O \approx -1.4$ per mil for O^+ and $\Delta^{17}O \approx 1.7$ per mil for O_2^+ at 120 km. These values and signs are related to those of the neutral species: $\Delta^{17}O \approx -2.0$ per mil for O and $\Delta^{17}O \approx 2.2$ per mil for O_2. The negative MIF for O originates from the fact that the production rate of ^{18}O is higher than those of lighter oxygens. The positive MIF for O_2 is the counterpart, and these senses are directly introduced into ionic species. The respective source reactions for O^+ and O_2^+ are mainly those of O (i.e. J6, R11, and R5) and O_2 (i.e. J4, R3, and R19) at the altitude of interest.

Now, let us consider the isotopic effect of the charge exchange R19 between O^+ and O_2^+. If the oxygen isotope is written as $Q \equiv {}^{17}O$ or ^{18}O, there are two possible reactions: (i) $Q^+ + O_2 \rightarrow Q + O_2^+$ (charge transfer) or $QO^+ + O$ (isotope transfer), and (ii) $O^+ + OQ \rightarrow O + OQ^+$, $OQ^+ + O$ (charge transfer), $O_2^+ + Q$, or $O + QO^+$ (isotope transfer). We determined the branching ratio by permuting the transition states, such that it is 0.5 for the former reaction, while it is 0.25 ($O_2^+ + Q$) and 0.75 ($O + OQ^+$) for the latter reaction. We confirmed that the MIF is not produced for any species by this statically distributed partitioning. The rate coefficients of these reactions for ^{17}O and ^{18}O were calculated on the basis of transition state theory (TST). Here, the rate constant is assumed to be a function of the energy difference between the transition state and reactants along with the partition function. We also derived the requisite energies and the structure constants (normal vibrational or rotational constants) by conducting a quantum chemical calculation with the Gamess program package (Schmidt et al., 1993). The obtained rate constants relative to the non-substituted reaction are (i) 0.980 for $^{17}O^+ + O_2 \rightarrow$ products and 0.962 for $^{18}O^+ + O_2 \rightarrow$ products, and (ii) 0.874 for $O^+ + {}^{17}OO \rightarrow$ products and 0.858 for $O^+ + {}^{18}OO \rightarrow$ products. The former two reactions are fairly mass-dependent, ≈ -1 per mil, while the latter two have large MIFs, ≈ -55 per mil. The large MIFs could be due to the symetrical properties of the transition state $[OQO]^+$ of the isotope transfer channel. In spite of the above rigorous calculation, the obtained values of $\Delta^{17}O^+$ shown in Fig. 5 are very small, except for a weak negative MIF for O_2^+. We consider that the composition of OQ is too small in the thermosphere to cause isotopic fractionation of the reaction products.

Finally, we considered the isotopic effect of the atom exchange reaction R35 between O and O_2. Anderson et al. (1985) measured the rate coefficients of $^{18}O + O_2 \rightleftharpoons O + {}^{18}OO$ to be 2.9×10^{12} cm^3s^{-1} by means of a discharge-flow, modulated molecular beam mass spectrometer. Because of the abundance of O and O_2, this value is comparable to the ion-molecule reactions listed in Table 1. We used their data in our model but assumed the rate coefficients for ^{17}O and ^{18}O exchange reactions were the same. Note that the rate of the backward reaction should be halved on the basis of the number of reaction paths. The isotopic dependences, $0.508\exp(-16/T)$ for ^{17}O and $0.516\exp(-32/T)$

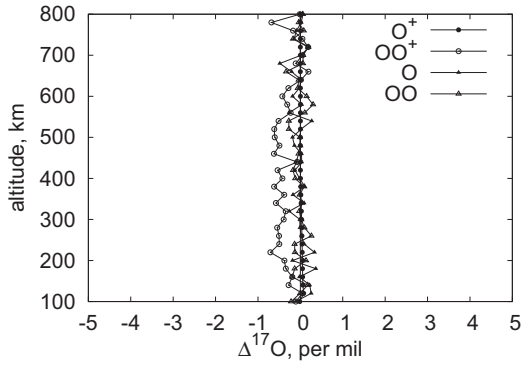

Fig. 5. Same as Fig. 2 except that the isotopic effect of the charge exchange reaction R19, $O^+ + O_2 \rightarrow O_2^+ + O$, is taken into account.

for ^{18}O, are taken from Navon and Wasserburg (1985). The results of the calculation are shown in Fig. 6. Δ^{17}O for O^+ and O are ≈1.4 and 2 per mil at 120 km, respectively. On the other hand, Δ^{17}O for O_2^+ and O_2 is negative, ≈−0.8 per mil, in the range of $z = 150$–600 km. The negative sign of Δ^{17}O for O_2 is related to the fact that the forward reaction rate for ^{17}OO is faster owing to the temperature dependence, and this leads to a massive amount of O_2. It is also related to the equivalence of the rate coefficient for ^{17}O and ^{18}O. The isotopic ratios of neutral species are directly converted into those of ionic species in a similar way to the case of Lyman-α photo-dissociation. Some calculations have varied the rate coefficient for ^{17}O within the experimental error range of ≈17% (Anderson et al., 1985), but these lead to no remarkable change from what is shown in Fig. 6. This implies that photolysis is still the dominant source and loss of O and O_2.

In summary, we investigated the isotopic effects of the key photolytic and chemical processes in the thermosphere, but obtained small values for the oxygen isotopic ratio, $\Delta^{17}O \approx \pm 1$–4 per mil. Chemical reactions do not produce strong isotopic fractionation for O^+ and other O-containing species. For the case of photolysis, although the obtained Δ^{17}O was not large, a rigorous quantum mechanical treatment of the photo-dissociation cross sections of J5 may end up giving a large MIF.

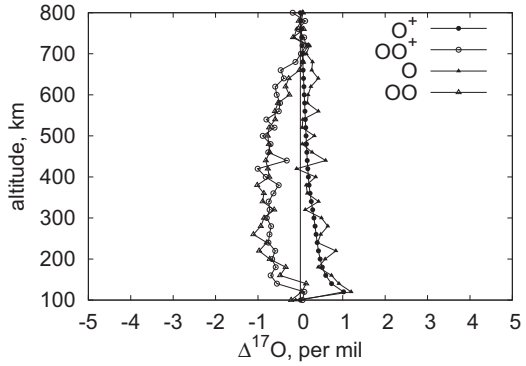

Fig. 6. Same as Fig. 2 except that the isotopic effect of the isotope exchange reaction R35, $O + O_2 \rightarrow O + O_2$, is taken into account.

4. DISCUSSION

In this section, we discuss the possibility of isotopic fractionation by processes that have not been addressed in our model. First let us comment on the lower boundary condition where the neutral species are supplied to the calculation region. The obtained results in Section 3 indicate that the peak altitude of Δ^{17}O for O^+ is around 100 km. Note that at this altitude molecular oxygen is effectively dissociated into O^+ by photolysis in the wavelength range of 50–100 nm. Since photon energies rapidly decrease below 100 km, the isotopic effects are at a maximum around this altitude even if other boundary conditions related to chemical losses are used. In this paper, we set the lower boundary at the point where $\Delta^{17}O = 0$ per mil for O and O_2 in order to examine the production of Δ^{17}O in the system. However, if the major component, or O_2, below 100 km is proved to have a large MIF, transport from the middle atmosphere may play a critical role in determining the thermospheric oxygen isotopic composition.

We should also point out the transport process in the rarefied weakly ionized atmosphere ($\geqslant$300 km). It is uncertain whether the calculated isotopic anomalies, mainly below 300 km, can spread to outer space and to the Moon without any modulation. This situation could be elucidated with a gas transport model that can treat the diffusion process in a non-equilibrium rarefied gas. Besides the transport process, the implantation process on the Moon should be addressed with regard to the effect of isotopic fractionation. These processes are similar to the transport of multiply-ionized atomic oxygen from the solar photosphere to the solar wind. Detailed studies have been made in association with the GENESIS spacecraft mission (Meshik et al., 2007). We can estimate these transport effects on the oxygen isotopic ratios by conducting a Monte Carlo test particle simulation including collisions of isotopes.

It is useful to monitor the progress of theoretical studies in photochemistry. In this study, we obtained the isotopic effects of two photolytic processes to produce a negative (red-shifted) $\Delta^{17}O = -1$–4 per mil for O^+. However, we cannot determine whether it is positive or negative, and the amplitudes, until we can make an exact evaluation of contributions of all absorption lines. The results may depend on the properties of the absorbers. It has been pointed out that the photo-dissociation rate coefficient for heavier O_2 may be higher than that for lighter O_2 due to the self-shielding effect of the oxygen-rich atmosphere (Cicerone and McCrumb, 1980; Navon and Wasserburg, 1985; Lyons and Young, 2005). We consider that the self-shielding is effective when there is an optical absorption line of mainly ^{18}O, and its contribution still appears in the integrated cross section. We should compile higher resolution photoionization cross sections of oxygen isotopes and elucidate the self-shielding effect on Δ^{17}O for O^+ in the terrestrial thermosphere. A detailed study is also necessary to determine the coupling between the dynamical and photolytic processes.

Finally, we suggest that comprehensive observations be made using a high resolution spectrometer in order to test our Earth-wind hypothesis for lunar oxygen isotopic anom-

alies. Although the resolution of the instrument itself would be less than 1 per mil, the experiment would have a lower resolution for passive satellite measurements of the upper atmosphere because of the slow sampling rate. A resolution of a few per mil would be needed to check the validity of our calculation's results. Spectroscopic measurements of the tropospheric and stratospheric ozone isotopes have been made by ground-based Fourier transform infrared (FTIR) instrumentation and by the ATMOS satellite with the FTIR solar occultation technique (see Mauersberger et al., 2005; Thiemens, 2006). The ozone isotopes were identified by these observations, but the spectral resolution was not high enough for our purposes. Furthermore, high sensitivity is needed in order to observe every absorption line of minor species in the upper atmosphere. We suppose that detailed information can be obtained by measuring strong emission lines of neutrals, O and NO, rather than direct measurements of O^+ emission lines. In that case though, a large ambiguity would still be involved in estimating the isotopic ratio of O^+ from the spectral data. Rocket-borne gas sampling measurements, as done by Thiemens et al. (1995), would be more accurate. Although detailed studies are needed to prove it, the Earth-wind hypothesis can at least offer a reasonable explanation for the amount of the exotic implanted oxygen isotopes in lunar metal (Ireland et al., 2006). Its validation would have far-reaching implications; for example, exotic oxygen would be able to be used as a unique tracer of the evolution of oxygen in the terrestrial atmosphere, which in turn would provide a new way to trace the appearance of life on Earth. We believe that the Earth-wind hypothesis deserves further examination and we urge that a search be conducted to determine the oxygen isotopic composition in the Earth wind.

5. SUMMARY

We developed a one-dimensional photochemical model that includes dynamical and chemical processes for oxygen isotopes in the terrestrial thermosphere. We performed several test simulations to estimate the isotopic fractionation rate of oxygen O^+ ions and took into account the isotopic effects of multi-diffusion processes, photo-dissociation of O_2, charge exchange between O^+ and O_2^+, and atomic exchange between O and O_2. We found that the oxygen isotopic ratio for O^+ as well as other species is mass dependent, i.e. $\Delta^{17}O \approx 0$ per mil, within the range of numerical errors by considering only diffusion processes. For the photolytic and chemical processes, we obtained a weak MIF, $\Delta^{17}O^+ \approx \pm 1$–4 per mil, and determined that most of the major chemical reactions cannot be the source of the MIF of Earth-escaping O^+. However, we do consider that photo-dissociation still has a possibility to produce a large MIF and we should evaluate its cross section data with a rigorous quantum mechanical treatment to find out if this is so. Although we are still at only the starting point of our investigation, this line of study is a fascinating chance for us to elucidate the relationship between the isotopic compositions of the Earth, the Moon, and the solar system.

REFERENCES

Anderson S. M., Klein F. S. and Kaufman F. (1985) Kinetics of the isotope exchange reaction of ^{18}O with NO and O_2 at 298 K. *J. Chem. Phys.* **83**(4), 1648–1656.

Bilitza D. (2001) International reference ionosphere 2000. *Radio Sci.* **36**(2), 261–275.

Boering K. A., Jackson T., Hoag K. J., Cole A. S., Perri M. J., Thiemens M. H. and Atlas E. (2004) Observations of the anomalous oxygen isotopic composition of carbon dioxide in the lower stratosphere and the flux of the anomaly to the troposphere. *Geophys. Res. Lett.* **31**, L03109, doi: 10.1029/2003GL018451.

Cicerone R. J. and McCrumb J. L. (1980) Photodissociation of isotopically heavy O_2 as a source of atmospheric 0_3. *Geophys. Res. Lett.* **7**, 251–254.

Clayton R. N. (2002a) Photochemical self-shielding in the solar nebula. *Lunar Planet. Sci.* XXXIII

Clayton R. N. (2002b) Solar system: self-shielding in the solar nebula. *Nature* **415**, 860–861.

DeMore W. B., Golden D. M., Hampson R. F., Howard C. J., Kurylo M. J., Molina M. J., Ravishankara A. R. and Sander S. P. (1994) Chemical Kinetics and Photochemical Data for Use in Stratospheric Modeling, Evaluation. Number 11, JPL Publication 94-26, Jet Propulsion Laboratory, California Institute of Technology, Pasadena, CA.

Gao Y. Q. and Marcus R. A. (2001) Strange and unconventional isotope effects in ozone formation. *Science* **293**, 259–263.

Hashizume K. and Chaussidon M. (2005) A non-terrestrial ^{16}O-rich isotopic composition for the protosolar nebula. *Nature* **434**, 619–622.

Hiraki Y., Kasai Y. and Fukunishi H. (2008a) Chemistry of sprite discharges through ion-neutral reactions. *Atmos. Chem. Phys.* **8**, 3919–3928.

Hiraki Y., Kasai Y., Ozima M., Seta T., Seki K. and Yamada A. (2008b) Terrestrial oxygen implanted on lunar soils by Earth Wind (EW). *Lunar Planet. Sci.* XXXIX, 1175

Ireland T. R., Holden P., Norman M. D. and Clarke J. (2006) Isotopic enhancements of ^{17}O and ^{18}O from solar wind particles in the lunar regolith. *Nature* **440**, 776–778.

Liang M.-C., Blake G. A., Lewis B. R. and Yung Y. L. (2007) Oxygen isotopic composition of carbon dioxide in the middle atmosphere. *PNAS* **104**, 21–25.

Lyons J. R. (2001) Transfer of mass-independent fractionation in ozone to other oxygen-containing radicals in the atmosphere. *Geophys. Res. Lett.* **28**, 3231–3234.

Lyons J. R. and Young E. D. (2005) CO self-shielding as the origin of oxygen isotope anomalies in the early solar nebula. *Nature* **435**, 317–320.

Mätzing H. (1991) Chemical kinetics and flue gas cleaning by irradiation with electrons. *Adv. Chem. Phys.* **80**, 315–402.

Mauersberger K., Krankowsky D., Janssen C. and Schinke R. (2005) Assessment of the ozone isotope effect. In *Adv. At. Mol. Opt. Phys.*, vol. 50 (eds. B. Bederson and H. Walther). Elsevier, Amsterdam.

Meshik A., Mabry J., Hohenberg C., Marrocchi Y., Pravdivtseva O., Burnett D., Olinger C., Wiens R., Reisenfeld D., Allton J., McNamara K., Stansbery E. and Jurewicz A. J. G. (2007) Constraints on neon and argon isotopic fractionation in solar wind. *Science* **19**, 433–435.

Navon O. and Wasserburg G. J. (1985) Self-shielding in O_2 – a possible explanation for oxygen isotopic anomalies in meteorites. *Earth Planet. Sci. Lett.* **73**, 1–16.

Ogawa T. and Shimazaki T. (1975) Diurnal variations of odd nitrogen and ionic densities in the me sosphere and lower thermosphere: simultaneous solution of photochemical-diffusive equations. *J. Geophys. Res.* **28**, 3945–3960.

Ozima M., Yin Q. -Z., Seki K., Podosek F. and Zahnle K. (2007) Biotic earth wind as the origin of oxygen isotope anomalies in contemporary lunar regolith. *Lunar Planet. Sci.* XXXVIII, 1129

Ozima M., Yin Q.-Z., Podosek F. A. and Miura Y. N. (2008) Toward understanding early Earth evolution: prescription for approach from terrestrial noble gas and light element records in lunar soils. *PNAS* **105**, 17654–17658.

Richards P. G., Fennelly J. A. and Torr D. G. (1994) EUVAC: a solar EUV flux model for aeronomic calculations. *J. Geophys. Res.* **99**(A5), 8981–8992.

Schmidt M. W., Baldridge K. K., Boatz J. A., Elbert S. T., Gordon M. S., Jensen J. H., Koseki S., Matsunaga N., Nguyen K. A., Su S., Windus T. L., Dupuis M. and Montgomery J. A. (1993) General atomic and molecular electronic structure system. *J. Comput. Chem.* **14**, 1347–1363.

Seki K., Elphic R. C., Hirahara M., Terasawa T. and Mukai T. (2001) On atmospheric loss of oxygen ions from Earth through magnetospheric processes. *Science* **291**, 1939–1941.

von Steiger R., Schwadron N. A., Fisk L. A., Geiss J., Gloeckler G., Hefti S., Wilken B., Wimmer-Schweingruber R. F. and Zurbuchen T. H. (2000) Composition of quasi-stationary solar wind flows from Ulysses/solar wind ion composition spectrometer. *J. Geophys. Res.* **105**(A12), 217–27,23, 27.

Thiemens M. H. (2006) History and applications of mass-independent isotope effects. *Annu. Rev. Earth Planet. Sci.* **34**, 217–262.

Thiemens M. H., Jackson T., Zipf E. C., Erdman P. W. and van Egmond C. (1995) Carbon dioxide and oxygen isotope anomalies in the mesosphere and stratosphere. *Science* **270**, 969–972.

Yamada A., Nanbu S., Hiraki Y., Seta T., Kasai Y. and Ozima M. (2009) Mass independent isotopic fractionation of oxygen in Earth wind (EW) with relevance to exotic oxygen in lunar metals. *Lunar Planet. Sci.* XXXX, 1478

Yung Y. L. and Miller C. E. (1997) Isotopic fractionation of stratospheric nitrous oxide. *Science* **278**, 1778–1780.

Yurimoto H. and Kuramoto K. (2004) Molecular cloud origin for the oxygen isotope heterogeneity in the solar system. *Science* **305**, 1763–1766.

MOLPRO is a package of ab initio programs written by H.-J. Werner and P.J. Knowles. Version 2006.1. See the MOLPRO homepage, <http://www.molpro.net>.

Zahn A., Franz P., Bechtel C., Groos J.-U. and Rockmann T. (2006) Modelling the budget of middle atmospheric water vapour isotopes. *Atmos. Chem. Phys.* **6**, 2073–2090.

Associate editor: James Farquhar